

Classical-quantum correspondence in bosonic two-mode conversion systems: polynomial algebras and Kummer shapes

H. J. Korsch

*FB Physik, TU Kaiserslautern, D-67653 Kaiserslautern, Germany**

(Dated: March 17, 2024)

Bosonic quantum conversion systems can be modeled by many-particle single-mode Hamiltonians describing a conversion of n m -atomic molecules into m n -atomic ones. These Hamiltonians are analyzed in terms of generators of a polynomially deformed $su(2)$ algebra. In the mean-field limit of large particle numbers, the system is classical and its Hamiltonian dynamics can again be described by a polynomial deformation of a Lie algebra, where quantum commutators are replaced by Poisson brackets. The Casimir operator restricts the motion to Kummer shapes, deformed Bloch spheres with cusp singularities depending on m and n . The many-particle state densities can be semiclassically approximated by the time-periods of periodic orbits, which show characteristic steps and singularities related to the fixed points, whose bifurcation properties are analyzed.

PACS numbers: 02.20.Sv, 03.65.Fd, 03.65.Sq, 05.30.Jp

I. INTRODUCTION

A recent paper by Graefe *et al.* [1] studies bosonic atom-molecule conversion systems describing (non-interacting) atoms which can undergo a conversion to diatomic molecules, both populating a single mode. This is the simplest possible conversion system modeling atom diatomic molecule conversion in cold atom systems and Bose-Einstein condensates (BECs). These systems have been studied extensively [2–14], quite often in a mean-field approximation [1, 3, 6, 7, 14] where the conversion can be described in terms of classical dynamics. In addition, the influence of particle interaction [6, 7, 10, 12, 15], noise [13] and particle losses [12] has been studied as well as extensions to systems coupling two modes [16].

The mean-field approximation of the many particle system derived in [1] based on a polynomially deformed $su(2)$ algebra [17–20] showed that the mean-field conversion dynamics takes place on a deformed Bloch sphere of a teardrop shape (see also [12]). Such surfaces also appear in different context, namely coupled classical harmonic oscillators at a 1 : 2 resonance which have been denoted as Kummer shapes [21, 22], named after preceding work by Kummer [23–27].

Here we extend the work in [1] to more general conversion systems, where m molecules consisting of n atoms can form a number n of m -atomic molecules and vice versa, conserving the number N of atoms. The corresponding Hamiltonian discussed in the subsequent section models, e.g., triatomic and tetratomic homonuclear molecular BECs [11], however, in addition to these applications in cold atom physics, it also describes other systems of interest in different areas of physics, as for example higher order harmonic generation, multiphoton processes, frequency conversion or, quite generally, the superposition of two harmonic oscillators.

For such systems, nonlinear polynomial algebras [17, 18, 28] arise in a natural way [2, 4, 8, 20, 29–32]. However they have been almost exclusively employed in context with superintegrability (or supersymmetry) [29–31] allowing an analytic evaluation of the energy spectrum by means of an algebraic Bethe ansatz [5, 11, 32]. Here we employ this algebraic approach to demonstrate an interesting connection between these quantum nonlinear algebras to corresponding ones in classical mechanics where quantum commutators are replaced by Poisson brackets in a mean-field approximation for large N . Here the general $n:m$ -Kummer shapes [21, 22] replace the celebrated Bloch sphere of the 1:1 case.

Algebraic methods are employed in most studies of many-particle conversion models, as for example the combined Heisenberg-Weyl and $su(1,1)$ algebras in [14] for atom-diatom conversion. Here we will employ polynomially deformed algebras appearing in a Jordan-Schwinger transformation, which is described in the following section. The corresponding mean-field system is derived in the subsequent section followed by a numerical comparison between mean-field and many-particle energies as well as state densities. We end with a summary and an outlook.

II. QUANTUM MANY-PARTICLE CONVERSION SYSTEMS

A toy model for studying multi-particle conversion systems is provided by the Hamiltonian

$$\hat{H}' = \epsilon_a \hat{a}^\dagger \hat{a} + \epsilon_b \hat{b}^\dagger \hat{b} + \frac{v}{2\sqrt{N^{m+n-2}}} (\hat{a}^\dagger \hat{m} \hat{b}^n + \hat{a}^m \hat{b}^{\dagger n}), \quad (1)$$

which describes a system of two types of ‘molecules’ A and B each consisting of n respectively m equal particles, or ‘atoms’, with creation and annihilation operators \hat{a}^\dagger , \hat{a} and \hat{b}^\dagger , \hat{b} , respectively, with $[\hat{a}, \hat{a}^\dagger] = [\hat{b}, \hat{b}^\dagger] = 1$, $[\hat{a}, \hat{b}] = [\hat{a}, \hat{b}^\dagger] = 0$, which can undergo a conversion, where m molecules of type A form n molecules of type B and vice

*Electronic address: korsch@physik.uni-kl.de

versa. (It is also possible to include additional interaction terms $\hat{a}^\dagger \hat{a} \hat{a}^\dagger \hat{a}$, $\hat{b}^\dagger \hat{b} \hat{b}^\dagger \hat{b}$ and $\hat{a}^\dagger \hat{a} \hat{b}^\dagger \hat{b}$ [6, 7, 10], but this is not considered here.) The total number N of particles

$$\hat{N} = n\hat{a}^\dagger \hat{a} + m\hat{b}^\dagger \hat{b} \quad (2)$$

is conserved: $[\hat{H}', \hat{N}] = 0$. In (1), $\epsilon_{a,b}$ are the energies of the molecular modes and v describes the conversion strength per particle, and, due to the N -dependent scaling factor of the conversion strength, all terms in the Hamiltonian scale linearly with N .

A. Quantum polynomial algebras

The analysis of the system described by the Hamiltonian (1) is greatly simplified by using techniques recently developed as deformed Lie algebras, more precisely polynomial deformations of the $su(2)$ algebra. Here we will closely follow the analysis by Lee *et al.* [20]. We first introduce the generalized Jordan-Schwinger mapping to the operators

$$\begin{aligned} \hat{s}_x &= \frac{\hat{a}^\dagger m \hat{b}^n + \hat{a}^m \hat{b}^\dagger n}{2\sqrt{N^{m+n-2}}}, \quad \hat{s}_y = \frac{\hat{a}^\dagger m \hat{b}^n - \hat{a}^m \hat{b}^\dagger n}{2i\sqrt{N^{m+n-2}}}, \\ \hat{s}_z &= \frac{n\hat{a}^\dagger \hat{a} - m\hat{b}^\dagger \hat{b}}{2mn} \end{aligned} \quad (3)$$

which commute with the number operator \hat{N} in (2). All these operators scale linearly with the particle number N .

Using the well known properties of the oscillator algebra one obtains the commutator

$$[\hat{a}^m, \hat{a}^{\dagger m}] = \Pi_{\mu=1}^m (\hat{a}^\dagger \hat{a} + \mu) - \Pi_{\mu=1}^m (\hat{a}^\dagger \hat{a} + 1 - \mu), \quad (4)$$

which is a polynomial of the number operator $\hat{a}^\dagger \hat{a}$ whose leading order term is

$$[\hat{a}^m, \hat{a}^{\dagger m}] = m^2 (\hat{a}^\dagger \hat{a})^{m-1} + \dots \quad (5)$$

We define a polynomial of order $m+n$ in \hat{N}' and \hat{s}_z , namely

$$\hat{P}(\hat{s}_z) = \Pi_{\mu=1}^m (\hat{N}' + \hat{s}_z + \frac{\mu}{m}) \Pi_{\nu=1}^n (\hat{N}' - \hat{s}_z - 1 + \frac{\nu}{n}), \quad (6)$$

where $\hat{N}' = \frac{\hat{N}}{2mn}$ is a rescaled number operator, with

$$\hat{P}(\hat{s}_z) \longleftrightarrow \hat{P}(-\hat{s}_z - 1) \quad \text{for } (m, n) \longleftrightarrow (n, m) \quad (7)$$

as well as the operator functions

$$\hat{F}(\hat{s}_z) = -d_m d_n (\hat{P}(\hat{s}_z) - \hat{P}(\hat{s}_z - 1)), \quad (8)$$

$$\hat{G}(\hat{s}_z) = -d_m d_n (\hat{P}(\hat{s}_z) + \hat{P}(\hat{s}_z - 1)). \quad (9)$$

with $d_k = k^k / \sqrt{2} N^{k-1}$. From (7) we find

$$\hat{F}(\hat{s}_z) \longleftrightarrow -\hat{F}(-\hat{s}_z), \quad \hat{G}(\hat{s}_z) \longleftrightarrow \hat{G}(-\hat{s}_z) \quad (10)$$

for $(m, n) \longleftrightarrow (n, m)$ and therefore for $m = n$ the symmetries

$$\hat{F}(-\hat{s}_z) = -\hat{F}(\hat{s}_z) \quad \text{and} \quad \hat{G}(-\hat{s}_z) = \hat{G}(\hat{s}_z), \quad (11)$$

i.e. $\hat{F}(\hat{s}_z)$ and $\hat{G}(\hat{s}_z)$ are odd or even polynomials.

According to [20], the commutation relations can be written as

$$[\hat{s}_z, \hat{s}_x] = i\hat{s}_y, \quad [\hat{s}_y, \hat{s}_z] = i\hat{s}_x, \quad [\hat{s}_x, \hat{s}_y] = i\hat{F}(\hat{s}_z) \quad (12)$$

(see also appendix A) and

$$\hat{C} = \hat{s}_x^2 + \hat{s}_y^2 + \hat{G}(\hat{s}_z) \quad (13)$$

is a Casimir operator commuting with all \hat{s}_j . Obviously this operator can be modified by adding terms depending only on the number operator \hat{N} , which also commutes with the \hat{s}_j .

The leading order term of the polynomials $\hat{P}(\hat{s}_z)$ and $\hat{P}(\hat{s}_z - 1)$ is equal to $(-1)^{n+1} \hat{s}_z^{(m+n)}$ and hence $\hat{G}(\hat{s}_z)$ or $\hat{F}(\hat{s}_z)$ are polynomials in \hat{s}_z of order $m+n$ or $m+n-1$, respectively.

In terms of the operators (3) we have

$$\hat{a}^\dagger \hat{a} = m(\hat{N}' + \hat{s}_z), \quad \hat{b}^\dagger \hat{b} = n(\hat{N}' - \hat{s}_z) \quad (14)$$

and the Hamiltonian (1) can be rewritten as

$$\hat{H}' = \hat{H} + (m\epsilon_a + n\epsilon_b)\hat{N}' \quad (15)$$

where, dropping the last term,

$$\hat{H} = \epsilon \hat{s}_z + v \hat{s}_x \quad \text{with} \quad \epsilon = m\epsilon_a - n\epsilon_b \quad (16)$$

is the Hamiltonian referred to in the following.

The Heisenberg equations of motion $i\dot{A} = [\hat{A}, \hat{H}]$ for the operators (3) read

$$\frac{d\hat{s}_x}{dt} = -\epsilon \hat{s}_y, \quad \frac{d\hat{s}_y}{dt} = \epsilon \hat{s}_x - v \hat{F}(\hat{s}_z), \quad \frac{d\hat{s}_z}{dt} = v \hat{s}_y \quad (17)$$

which conserve, in addition to the particle number \hat{N} , the Casimir operator $\hat{C}(\hat{s}_x, \hat{s}_y, \hat{s}_z)$, i.e.

$$\hat{s}_x^2 + \hat{s}_y^2 = \hat{C} - \hat{G}(\hat{s}_z), \quad (18)$$

and therefore $\langle \hat{s}_x^2 \rangle + \langle \hat{s}_y^2 \rangle = \langle \hat{C} \rangle - \langle \hat{G}(\hat{s}_z) \rangle$ corresponding to a generalized Bloch sphere [13], i.e. a deformation of the Bloch sphere also denoted as a quantum Kummer shape [33] in view of the classical Kummer shapes discussed in the mean-field approximation in section III.

For later reference we evaluate the leading terms in the limit of large N . With the abbreviations $\hat{A}_\pm = \hat{N}' \pm \hat{s}_z$ one obtains from (6) and (8), (9)

$$\hat{P}(\hat{s}_z) = \hat{A}_+^m \hat{A}_-^n - \frac{n-1}{2} \hat{A}_+^m \hat{A}_-^{n-1} + \frac{m+1}{2} \hat{A}_+^{m-1} \hat{A}_-^n + \dots \quad (19)$$

$$\hat{P}(\hat{s}_z - 1) = \hat{A}_+^m \hat{A}_-^n + \frac{n+1}{2} \hat{A}_+^m \hat{A}_-^{n-1} - \frac{m-1}{2} \hat{A}_+^{m-1} \hat{A}_-^n + \dots \quad (20)$$

and

$$\hat{F}(\hat{s}_z) = d_m d_n (n \hat{A}_+^m \hat{A}_-^{n-1} - m \hat{A}_+^{m-1} \hat{A}_-^n + \dots) \quad (21)$$

$$\hat{G}(\hat{s}_z) = -d_m d_n (\hat{A}_+^m \hat{A}_-^n + \dots). \quad (22)$$

Let us discuss some cases considered in the following section in more detail, where in view of the symmetry (10) it is sufficient to study the cases $m \geq n$.

(1) $(m, n) = (1, 1)$: In this linear case we encounter the $su(2)$ algebra, namely

$$\hat{P}(\hat{s}_z) = -\hat{s}_z^2 - \hat{s}_z + \hat{N}'^2 + \hat{N}' \quad (23)$$

$$\hat{P}(\hat{s}_z - 1) = -\hat{s}_z^2 + \hat{s}_z + \hat{N}'^2 + \hat{N}' \quad (24)$$

and, with $d_1^2 = 1/2$, we have

$$\hat{F}(\hat{s}_z) = \hat{s}_z, \quad \hat{G}(\hat{s}_z) = \hat{s}_z^2 - \hat{N}'^2 - \hat{N}' \quad (25)$$

and the Casimir operator is

$$\hat{C} = \hat{s}_x^2 + \hat{s}_y^2 + \hat{s}_z^2 - \hat{N}'^2 - \hat{N}'. \quad (26)$$

Up to insignificant \hat{N}' -dependent terms this operator is known as \hat{L}^2 for the angular momentum algebra. The Casimir operator imposes a restriction to the surface of a sphere, the Bloch sphere

$$\hat{s}_x^2 + \hat{s}_y^2 = \hat{C} + \hat{N}'^2 + \hat{N}' - \hat{s}_z^2. \quad (27)$$

(2) $(m, n) = (2, 1)$: In this case, describing a conversion of two ‘atoms’ into diatomic ‘molecules’, which has been studied quite extensively (see [1] and references therein), we have

$$\begin{aligned} \hat{P}(\hat{s}_z) = & -\hat{s}_z^3 - (\hat{N}' + \frac{3}{2})\hat{s}_z^2 + (\hat{N}'^2 - \frac{1}{2})\hat{s}_z \\ & + \hat{N}'^3 + \frac{3}{2}\hat{N}'^2 + \frac{1}{2}\hat{N}' \end{aligned} \quad (28)$$

$$\begin{aligned} \hat{P}(\hat{s}_z - 1) = & -\hat{s}_z^3 - (\hat{N}' - \frac{3}{2})\hat{s}_z^2 + (\hat{N}'^2 + 2\hat{N}' - \frac{1}{2})\hat{s}_z \\ & + \hat{N}'^3 + \frac{1}{2}\hat{N}'^2 - \frac{1}{2}\hat{N}' \end{aligned} \quad (29)$$

and, with $d_1 d_2 = 2/N$,

$$\hat{F}(\hat{s}_z) = \frac{6}{N}\hat{s}_z^2 + \frac{\hat{N}}{N}\hat{s}_z - \frac{\hat{N}^2}{8N} - \frac{\hat{N}}{2N}, \quad (30)$$

$$\hat{G}(\hat{s}_z) = \frac{4}{N}\hat{s}_z^3 + \frac{\hat{N}}{N}\hat{s}_z^2 + \frac{8 - \hat{N}^2 - 4\hat{N}}{4N}\hat{s}_z - \frac{4\hat{N}^3}{N} + \frac{4\hat{N}^2}{N} \quad (31)$$

in agreement with [1] up to the \hat{s}_z -independent terms.

(3) $(m, n) = (2, 2)$: For this case the nonlinear algebra corresponds to the (cubic) Higgs algebra (see [29, 31] and references therein) with

$$\hat{P}(\hat{s}_z) = \hat{s}_z^4 + 2\hat{s}_z^3 - (2\hat{N}'^2 + \hat{N}' - \frac{5}{4})\hat{s}_z^2 \quad (32)$$

$$- (2\hat{N}'^2 + \hat{N}' - \frac{1}{4})\hat{s}_z + \hat{N}'^4 + \hat{N}'^3 - \frac{1}{4}\hat{N}'^2 - \frac{1}{4}\hat{N}'$$

$$\hat{P}(\hat{s}_z - 1) = \hat{P}(-\hat{s}_z) \quad (33)$$

and, with $d_2^2 = 8/N^2$,

$$\hat{F}(\hat{s}_z) = \frac{4}{N^2}(-8\hat{s}_z^3 + (8\hat{N}'^2 + 4\hat{N}' - 1)\hat{s}_z) \quad (34)$$

$$\begin{aligned} \hat{G}(\hat{s}_z) = & \frac{4}{N^2}(-4\hat{s}_z^4 + (8\hat{N}'^2 + 4\hat{N}' - 5)\hat{s}_z^2 \\ & - 4\hat{N}'^4 - 4\hat{N}'^3 + \hat{N}'^2 + \hat{N}'). \end{aligned} \quad (35)$$

Note that $\hat{F}(\hat{s}_z)$ is an odd polynomial in \hat{s}_z and $\hat{G}(\hat{s}_z)$ is even, as stated in (11).

In the same way the cases $m, n \geq 3$ can be rewritten as explicit polynomials, if desired. It should be noted that the relations between the polynomials $\hat{F}(\hat{s}_z)$ and $\hat{G}(\hat{s}_z)$ for all these cases agree with equation (A9) in the appendix, interrelating the coefficients of the polynomials.

B. Numerical calculations

The dimension of the Hilbert space is $N_{\text{dim}} = \frac{N}{mn} + 1$ where we will assume in the following that N is an integer multiple of mn . As a consequence of the superintegrability the eigenvalues of the Hamiltonians can be obtained analytically [11, 20] by means of a Bethe ansatz [32], but for the following results we simply diagonalize \hat{H} numerically using a Fock basis

$$|j\rangle = \frac{1}{\sqrt{j!}} \hat{a}^{\dagger j} |0\rangle, \quad j = 0, 1, \dots \quad (36)$$

with $\langle j' | j \rangle = \delta_{j', j}$ and

$$\begin{aligned} \langle j' | \hat{a}^\dagger \hat{a} | j \rangle &= j \delta_{j', j}, \quad \langle j' | \hat{a}^{\dagger m} | j \rangle = \sqrt{\frac{(j+m)!}{j!}} \delta_{j', j+m}, \\ \langle j' | \hat{a}^m | j \rangle &= \sqrt{\frac{j!}{(j-m)!}} \delta_{j', j-m} \end{aligned} \quad (37)$$

and similarly for \hat{b} with j replaced by k . The states $|j, k\rangle$ form an orthonormal basis of the Hilbert space. The N_{dim} -dimensional subspaces of eigenstates of \hat{N} with eigenvalue N are spanned by the basis

$$|\mu\rangle = |\mu m, \frac{N}{m} - \mu n\rangle, \quad \mu = 0, 1, \dots, \frac{N}{mn}. \quad (38)$$

Then the operators $\hat{s}_x, \hat{s}_y, \hat{s}_z$ are represented by the matrices

$$\langle \mu' | \hat{s}_x | \mu \rangle = \frac{1}{2}(\sqrt{\beta_{\mu+1}} \delta_{\mu', \mu+1} + \sqrt{\beta_\mu} \delta_{\mu', \mu-1}), \quad (39)$$

$$\langle \mu' | \hat{s}_y | \mu \rangle = \frac{1}{2i}(\sqrt{\beta_{\mu+1}} \delta_{\mu', \mu+1} - \sqrt{\beta_\mu} \delta_{\mu', \mu-1}), \quad (40)$$

$$\langle \mu' | \hat{s}_z | \mu \rangle = (\mu - \frac{N}{2mn}) \delta_{\mu', \mu}. \quad (41)$$

with $\beta_\mu = N^{2-m-n}(\mu m - m + 1) \cdots (\mu m)(N/m - \mu n + 1) \cdots (N/m - \mu n + n)$. The matrices representing \hat{s}_x and \hat{s}_y are tridiagonal and the matrix \hat{s}_z is diagonal with equidistant eigenvalues ranging from $-\frac{N}{2mn}$ for $\mu = 0$ to $+\frac{N}{2mn}$ for $\mu = \frac{N}{mn}$. Trivially \hat{N} is equal to the identity multiplied by N , so that also $\hat{F}(\hat{s}_z)$ and $\hat{G}(\hat{s}_z)$ are diagonal.

III. CLASSICAL MEAN-FIELD SYSTEMS

In the mean-field limit $N \rightarrow \infty$, also denoted as thermodynamic limit, the quantum operators as $\hat{A}(\hat{a}, \hat{a}^\dagger)$ are replaced by c functions $A(a, a^*)$ and the quantum commutator $[\hat{A}, \hat{B}]$ by the Poisson bracket $\{A, B\} =$

$\partial_a A \partial_{a^*} B - \partial_a B \partial_{a^*} A + \partial_b A \partial_{b^*} B - \partial_b B \partial_{b^*} A$. In order to derive this thermodynamic limit for the systems discussed above, we follow two different routes:

(a) First, as done by Graefe *et al.*, [1], we consider the limit $\eta = (\frac{N}{mn} + 1)^{-1} \rightarrow 0$, where only the leading order terms of the algebra survive. With $\eta \hat{A} \rightarrow A$ and $\eta^2 [\hat{A}, \hat{B}] \rightarrow i\{A, B\}$ the commutator relations (12) transform to

$$\{s_z, s_x\} = s_y, \quad \{s_y, s_z\} = s_x, \quad \{s_x, s_y\} = f(s_z) \quad (42)$$

and, with $\eta \hat{K}_j \rightarrow s_j$, $\eta \hat{N} \rightarrow mn$ and $\eta \hat{N}' \rightarrow \frac{1}{2}$, we have

$$\eta \frac{\hat{A}_+^m \hat{A}_-^{n-1}}{N^{m+n-2}} \rightarrow (mn)^{2-m-n} \left(\frac{1}{2} + s_z\right)^m \left(\frac{1}{2} - s_z\right)^{n-1} \quad (43)$$

$$\eta^2 \frac{\hat{A}_+^m \hat{A}_-^n}{N^{m+n-2}} \rightarrow (mn)^{2-m-n} \left(\frac{1}{2} + s_z\right)^m \left(\frac{1}{2} - s_z\right)^n \quad (44)$$

and finally from (21) $\eta \hat{F}(\hat{s}_z) \rightarrow f(s_z)$ and $\eta^2 \hat{G}(\hat{s}_z) \rightarrow g(s_z)$ with

$$f(s_z) = \frac{1}{2} m^{2-n} n^{2-m} \left(n \left(\frac{1}{2} + s_z\right)^m \left(\frac{1}{2} - s_z\right)^{n-1} - m \left(\frac{1}{2} + s_z\right)^{m-1} \left(\frac{1}{2} - s_z\right)^n \right) \quad (45)$$

$$g(s_z) = -m^{2-n} n^{2-m} \left(\frac{1}{2} + s_z\right)^m \left(\frac{1}{2} - s_z\right)^n, \quad (46)$$

i.e according to (13) we obtain $\eta^2 \hat{C} \rightarrow C$ with

$$C(s_x, s_y, s_z) = s_x^2 + s_y^2 + g(s_z). \quad (47)$$

For the special case $(m, n) = (2, 1)$ this yields

$$f(s_z) = -\frac{1}{4} + s_z + 3s_z^2 \quad (48)$$

$$g(s_z) = -\frac{1}{4} - \frac{1}{4}s_z + s_z^2 + 2s_z^3 \quad (49)$$

in agreement with [1].

(b) Alternatively, one can start from the classicalized version of the Hamiltonian (1),

$$H' = \epsilon_a a^* a + \epsilon_b b^* b + v' (a^{*m} b^n + a^m b^{*n}), \quad (50)$$

where the operators \hat{a}, \hat{a}^\dagger are replaced by c-numbers a, a^* , i.e. $\eta \hat{a} \hat{a}^\dagger \rightarrow a^* a$ with $\{a, a^*\} = -i$. The equations of motion $\dot{A} = \{A, H'\}$ conserve the function $na^* a + mb^* b$, whose value is the limit $\eta(n\hat{a}^\dagger \hat{a} + m\hat{b}^\dagger \hat{b}) = \eta \hat{N} \rightarrow mn$. In analogy to (3) we define

$$s_x = \frac{a^{*m} b^n + a^m b^{*n}}{2\sqrt{(nm)^{m+n-2}}}, \quad s_y = \frac{a^{*m} b^n - a^m b^{*n}}{2i\sqrt{(nm)^{m+n-2}}}, \quad (51)$$

$$s_z = \frac{na^* a - mb^* b}{2mn}.$$

with

$$a^* a = m\left(\frac{1}{2} + s_z\right) \quad \text{and} \quad b^* b = n\left(\frac{1}{2} - s_z\right) \quad (52)$$

in correspondence with (14).

The Poisson bracket relations and the Casimir function can be easily evaluated using $\{a, a^{*m}\} = -ima^{*m-1}$ as well as

$$\{a^m, a^{*m}\} = -im^2(a^* a)^{m-1} \quad (53)$$

in agreement with the leading order term (5) of the quantum commutator, and can be found in Holm's book *Geometric Mechanics* [21]. The results are again the Poisson brackets (42) with the same function $f(s_z)$ obtained in (45) and finally from (51) and (52)

$$s_x^2 + s_y^2 = (mn)^{2-m-n} (a^* a)^m (b^* b)^n = m^{2-n} n^{2-m} \left(\frac{1}{2} + s_z\right)^m \left(\frac{1}{2} - s_z\right)^n = -g(s_z), \quad (54)$$

which defines the functional relation $C(s_x, s_y, s_z) = s_x^2 + s_y^2 + g(s_z)$ [21], exactly as obtained above.

A. Classical polynomial algebras

We therefore obtain the Poisson bracket relations

$$\{s_z, s_x\} = s_y, \quad \{s_y, s_z\} = s_x, \quad \{s_x, s_y\} = f(s_z) \quad (55)$$

and we defined the function

$$C(s_x, s_y, s_z) = s_x^2 + s_y^2 + g(s_z), \quad (56)$$

where $f(s_z)$ and $g(s_z)$ are given in (45) and (46). One can easily check that these functions satisfy

$$\frac{dg(s_z)}{ds_z} = 2f(s_z) \quad (57)$$

and therefore we find, using $\{s_x, h(s_z)\} = -s_y h'(s_z)$ and $\{s_y, h(s_z)\} = s_x h'(s_z)$, the relations

$$\{C, s_x\} = \{C, s_y\} = \{C, s_z\} = 0. \quad (58)$$

This is a polynomial deformation of the Lie algebra with a Poisson bracket instead of a commutator and the Casimir function $C(s_x, s_y, s_z)$, i.e. it is a constant of motion for Hamiltonians $H(s_x, s_y, s_z)$.

B. Dynamics on Kummer shapes

The vector $\mathbf{s} = (s_x, s_y, s_z)$ evolves in time according to the equations of motion (62) keeping the Casimir function constant, $C(\mathbf{s}) = C$, where the value C can be chosen equal to zero. An immediate consequence for a system with Hamiltonian $H(\mathbf{s})$ is the restriction of the dynamics to the orbit manifold

$$s_x^2 + s_y^2 = -g(s_z) = r^2(s_z) = m^{2-n} n^{2-m} \left(\frac{1}{2} + s_z\right)^m \left(\frac{1}{2} - s_z\right)^n, \quad (59)$$

i.e. a surface of revolution with a s_z -dependent radius $r(s_z)$. Following Holm these surfaces will be denoted as

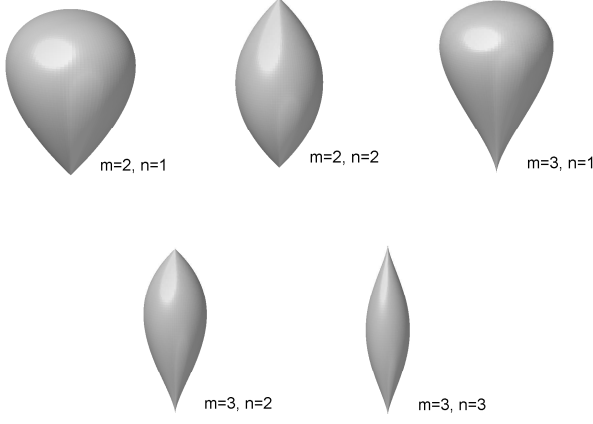


FIG. 1: Kummer shapes (59) for selected values of m and n .

Kummer shapes based on previous work by Kummer (see [21, 22, 25–27]), which generalizes the Bloch sphere

$$s_x^2 + s_y^2 = r^2(s_z) = \frac{1}{4} - s_z^2 \quad (60)$$

for $(m, n) = (1, 1)$ to polynomial algebras. Figure 1 shows some examples.

These Kummer shapes are manifolds with the possible exceptions of the poles $\mathbf{s}_\pm = (0, 0, \pm \frac{1}{2})$. Here the surface is smooth at the north pole \mathbf{s}_+ for $n = 1$, at the south pole \mathbf{s}_- for $m = 1$. For $n \geq 2$ or $m \geq 2$ the surfaces are pinched at these points, where we have a tip for m or n equal to 2 and a cusp for larger values. Figure 2 shows the radius $r(s_z)$ as a function of s_z for selected m and n . The slope of the radius $r(s_z)$ at the poles is infinite for n or m equal to 1, for $m = 2$ the slope at \mathbf{s}_- is equal to $2^{1-n/2}$, i.e. $\sqrt{2}$ for $n = 1$, 1 for $n = 2$ and $1/2$ for $n = 4$. For $n = 2$ the slope at \mathbf{s}_+ is equal to $2^{1-m/2}$. For $m, n > 2$ the slope at the poles is zero.

Let us recall that the dynamics generated by the Hamiltonian

$$H = v s_x + \epsilon s_z \quad (61)$$

follows the equations of motion $\dot{s}_j = \{s_j, H\}$, i.e.

$$\dot{s}_x = -\epsilon s_y, \quad \dot{s}_y = \epsilon s_x - v f(s_z), \quad \dot{s}_z = v s_y \quad (62)$$

and the conservation of $C(s_x, s_y, s_z)$ restricts the orbit to the Kummer surface (59), and in addition by the conservation of energy, so that the orbits are geometrically given by the intersection of the Kummer shape (59) with the surface $H(s_x, s_y, s_z) = E$, which is a plane for the Hamiltonian (50).

As already pointed out in Holm's book [21] as well as in [33], the Kummer dynamics can be formulated in terms of the Nambu-Poisson bracket, a Lie bracket which also satisfies the Leibnitz relation [34]. Using the relation (57)

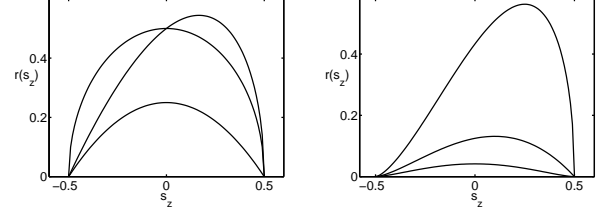


FIG. 2: Radius $r(s_z)$ of the Kummer surface (59) for $(m, n) = (1, 1), (2, 1), (2, 2)$ (left) and $(3, 1), (3, 2), (3, 3)$ (right).

between $f(s_z)$ and $g(s_z)$, one can rewrite the equations of motions in terms of the Nambu bracket

$$\{A, B\}_C = \frac{1}{2} \nabla C \cdot (\nabla A \times \nabla B), \quad (63)$$

where $\frac{1}{2} \nabla C = (s_x, s_y, f(s_z))$ is the gradient of the Casimir function given in (56), in the convenient form

$$\dot{A} = \{A, H\}_C, \quad (64)$$

which immediately reveals the conservation of both the Hamiltonian H and the Casimir function C . In addition, the equation of motion for the vector \mathbf{s} can be written as

$$\dot{\mathbf{s}} = \{\mathbf{s}, H\}_C = \frac{1}{2} \nabla C \times \nabla H. \quad (65)$$

Alternatively, one can describe the dynamics in terms of canonical variables p and q , where p is equal to s_z and q is the angle in the s_x, s_y plane [1]:

$$s_z = p, \quad s_x = r(p) \cos q, \quad s_y = r(p) \sin q \quad (66)$$

with radius (compare (59))

$$r(p) = r_0 \left(\frac{1}{2} + p\right)^{m/2} \left(\frac{1}{2} - p\right)^{n/2}, \quad r_0 = m^{1-n/2} n^{1-m/2}. \quad (67)$$

Then the dynamics is given by the standard Poisson bracket $\{A, B\} = \partial_p A \partial_q B - \partial_q A \partial_p B$ and the Hamiltonian

$$H(p, q) = \epsilon p + v r(p) \cos q. \quad (68)$$

Note that in this formulation the restriction to the Kummer surface (59) is immediately obvious.

Furthermore this canonical description can be conveniently used as a basis for a semiclassical WKB-type quantization recovering the individual multi-particle energy eigenvalues and eigenstates from the mean-field as carried out for $(m, n) = (1, 1)$ in [35–37] and for $(m, n) = (2, 1)$ in [1]. This quantization condition reads

$$S(\eta E_\nu) = 2\pi\eta(\nu + \frac{1}{2}) \quad (69)$$

where $S(E)$ is the phase space area enclosed by the orbit of energy E .

Here we will confine ourselves to the density of states and extend the analysis of previous work [1, 35] to general

values of m and n . The many-particle density of states $\rho(E)$ at a scaled energy E is (approximately) related to the mean-field period $T(E) = dS/dE$ of the orbit by

$$\rho(E) \approx \frac{1}{2\pi} T(E) = \frac{1}{\pi} \int_{p_-}^{p_+} \frac{dp}{\sqrt{(U_+(p) - E)(E - U_-(p))}}, \quad (70)$$

where

$$U_{\pm}(p) = \epsilon p \pm v r(p) \quad (71)$$

are momentum-dependent potential curves with $U_+(\pm\frac{1}{2}) = U_-(\pm\frac{1}{2}) = \pm\frac{\epsilon}{2}$ and p_{\pm} are the turning points, the real valued solutions of $U_{\pm}(p) = E$ falling into the interval $[-\frac{1}{2}, +\frac{1}{2}]$. The function under the square root in (70),

$$(U_+(p) - E)(E - U_-(p)) = v^2 r^2(p) - (E - \epsilon p)^2, \quad (72)$$

is a polynomial of order $m+n$ in p and the integral (70) can be evaluated in closed form for $(m, n) = (1, 1)$ and $(m, n) = (2, 1)$ [1, 35].

Numerical examples of the mean-field approximation in comparison with the quantum many-particle density are presented in section IV.

C. Fixed points

Important for the organization of the dynamics both in classical and quantum mechanics are the fixed points of the motion. The fixed points are found at $s_y = 0$ and $\epsilon s_x = v f(s_z)$. This is always satisfied at the poles $\mathbf{s}_{\pm} = (0, 0, \pm\frac{1}{2})$, so that the poles are fixed points for all parameter values, however their character can change from a center to a saddle.

The fixed point condition can be rewritten as $\epsilon^2 s_x^2 = v^2 f^2(s_z)$ or, using (59) and (45),

$$\begin{aligned} 16\epsilon^2 m^{n-2} n^{m-2} \\ = v^2 \left(\frac{1}{2} + s_z\right)^{m-2} \left(\frac{1}{2} - s_z\right)^{n-2} (2(n+m)s_z + n - m)^2. \end{aligned} \quad (73)$$

The real roots of this polynomial of degree $m+n-2$ with $-\frac{1}{2} \leq s_z \leq +\frac{1}{2}$, $s_x = v f(s_z)$, $s_y = 0$, yield the fixed points, whose character can be determined from the eigenvalues of the Jacobi matrix

$$\lambda_{\pm} = \pm \sqrt{-\epsilon^2 - v^2 f'(s_z)}, \quad (74)$$

which are a complex conjugate pair for a center, i.e. a rotation with frequency

$$\omega = \sqrt{\epsilon^2 + v^2 f'(s_z)} \quad (75)$$

or a pair of real numbers with different signs for a saddle point. Note that for $m = n$ the fixed point equation (73) simplifies to

$$\epsilon^2 m^{2m-4} = v^2 \left(\frac{1}{4} - s_z^2\right)^{m-2} s_z^2, \quad (76)$$

a polynomial of order $m-1$.

It is instructive to have a look at figure 2. At a fixed point the energy plane $E = v s_x + \epsilon s_z$ is tangential to the Kummer surface, i.e. the slope of the straight line $s_x = (E - \epsilon s_z)/v$ must be equal to the slope of $r(s_z)$. For $(m, n) = (1, 1)$, i.e. for the Bloch sphere, this can always be satisfied. For $m = 2$ or $n = 2$ the slope $r'(s_z)$ is bounded by the slope at $-\frac{1}{2}$ or $+\frac{1}{2}$, which is equal to $2^{n/2-1}$ or $2^{m/2-1}$, i.e. we have $\epsilon^2/v^2 \leq 2^{n-2}$ or $\epsilon^2/v^2 \leq 2^{m-2}$.

For $m, n > 2$ the slope at the poles is zero, so that $r'(s_z)$ has a maximum value at the point of inflection. One can easily show that there are only two such points of inflection, for the symmetric case $m = n$ located at $s_z = \pm 1/2\sqrt{m-1}$, with the consequence that there can be at most two points where $r'(s_z)$ has a prescribed value, i.e. two fixed points $\mathbf{s}_{1,2}$ with $s_x > 0$, and, because of symmetry, two additional ones at $-\mathbf{s}_{1,2}$.

At critical parameter values the number of fixed points changes. This can happen in two ways at ϵ_c :

(i) Two fixed points can coalesce and disappear. This saddle-node bifurcation must necessarily occur at the inflection point s_z of $r(s_z)$ and the critical value of ϵ is given by its slope as the slope at this point: $\epsilon_c = \pm v r'(s_z)$.

(ii) Fixed points can enter or leave the system at the poles in a transcritical bifurcation [1]. Because the slope of $r(s_z)$ at the poles is zero for $m, n > 2$, this can (for $\epsilon \neq 0$) only happen if m or n is equal to 2, for $m = 2$ at the south pole for $\epsilon_c = v 2^{1-n/2}$ and for $n = 2$ at the north pole for $\epsilon_c = v 2^{1-m/2}$. A stability analysis shows that here a center at the pole changes into a saddle and a new center appears moving away from the pole. In the parameter region $-\epsilon_c < \epsilon < \epsilon_c$ we have therefore three fixed points if only one of the m, n is equal to two or four if $m = n = 2$. Outside this region there are only two, namely the poles. For $\epsilon = 0$ and $m > 2$ the fixed point at the south pole is degenerate and bifurcates into a saddle and a center for $\epsilon \neq 0$, as well at the north pole for $n > 2$.

One should realize that the sum of the Poincaré indices (centers have index +1, saddles index -1, see, e.g., [38]) remains constant on the Kummer surface for bifurcations of type (i), whereas it changes for type (ii).

IV. MEAN-FIELD AND MANY-PARTICLE CORRESPONDENCE

Let us discuss the correspondence between quantum many-particle eigenvalues and mean-field dynamics for some cases in more detail. We will use the notation p, q introduced at the end of section III B. The allowed mean-field energy interval is bounded by the energies at the fixed points p_f , the real solutions of the polynomial (73) in the interval $[-\frac{1}{2}, +\frac{1}{2}]$, i.e. $E_{\pm} = \pm\epsilon/2$ for the fixed points at the poles or

$$E_j = \frac{v^2}{\epsilon} f(p_j) + \epsilon p_j \quad (77)$$

at the additional fixed points p_j , provided they exist, which are minima or maxima of the energy function (68). For large values of $|\epsilon|$, in the supercritical regime, where we have only two fixed points at the poles, the mean-field energy interval is $E_- < E < E_+$, and in the subcritical regime below the critical value(s) of ϵ , the upper or lower bound of the energy region is given by the energy (77).

The quantum state density $\rho(E)$ at an energy E can be approximately described by $T(E)/2\pi$ (compare (70)), where the mean-field period $T(E)$ given by the integral (70) can be efficiently evaluated by means of a Gauss-Mehler quadrature. If the fixed point is a center, $T(E)/2\pi$ is given by the inverse frequency $\omega = \sqrt{\epsilon^2 + v^2 f'(p_c)}$ at the center p_c (see (75)). In the subcritical parameter region, the period T diverges logarithmically at the saddle point energies, as already observed before for the Bloch sphere $m = n = 1$ [35, 39] and for $(m, n) = (2, 1)$ [1]. Therefore the quantum energy eigenvalues accumulate at the all-molecule configurations in this regime, as will be demonstrated by the examples below.

It is worthwhile to note that in all cases the eigenvalues are non-degenerate so that all apparent crossings are avoided as already observed before for an atom-molecule conversion system [5]. This, however is simply a consequence of the fact that the Hamiltonian is tridiagonal (see section II B) and hence can only have eigenvalue degeneracies if all off-diagonal elements vanish [40].

(1) For $(m, n) = (1, 1)$, i.e. for the dynamics on the Bloch sphere, we have $f(p) = p$ and the two fixed points are at $p_{\pm} = \pm 1/(2\sqrt{1 + v^2/\epsilon^2})$, $q_+ = 0$, $q_- = \pi$, which are both centers with frequency $\omega = \sqrt{\epsilon^2 + v^2}$ and an energy

$$E_{\pm} = H(p_{\pm}, q_{\pm}) = \pm \frac{1}{2} \sqrt{\epsilon^2 + v^2}. \quad (78)$$

Moreover one can easily show that *all* points move on circles with frequency ω . Consequently the quantum state density is approximately constant in the interval $E_- < E < E_+$.

(2) The case $(m, n) = (2, 1)$ has been analyzed in [1, 14]. Here the Kummer surface

$$\begin{aligned} s_x^2 + s_y^2 &= r^2(p) \\ &= 2\left(\frac{1}{2} + p\right)^2 \left(\frac{1}{2} - p\right) = \frac{1}{4} + \frac{1}{2}p - p^2 - 2p^3 \end{aligned} \quad (79)$$

has the shape of a teardrop. At the north pole it is smooth and there is a tip at the south pole. The slope of $r(p)$ at the south pole is equal to $\sqrt{2}$, which is the critical value of $\pm\epsilon/v$. Therefore the subcritical regime can be identified as $-\sqrt{2} < \epsilon/v < +\sqrt{2}$ (see also [1, 14]) and the supercritical one with only two fixed points at the poles otherwise. With $f(p) = -\frac{1}{4} + p + 3p^2$ the equations of motion written in terms of the \hat{s}_j are

$$\dot{s}_x = -\epsilon s_y, \quad \dot{s}_y = \epsilon s_x - v\left(-\frac{1}{4} + s_z + 3s_z^2\right), \quad \dot{s}_z = v s_y \quad (80)$$

and the equation for the z -component of the fixed points reads

$$\left(\frac{1}{2} + p\right)(9v^2p^2 + (2\epsilon^2 - 3v^2)p + \frac{v^2}{4} - \epsilon^2) = 0 \quad (81)$$

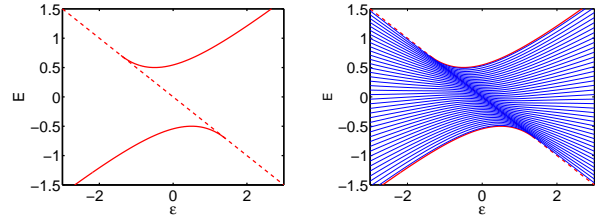


FIG. 3: $(m, n) = (2, 1)$: Mean-field fixed point energies (red) and (scaled) many-particle energies (blue) in dependence of ϵ for $v = 1$ and $N = 80$ particles.

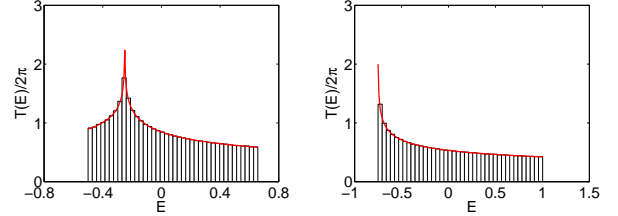


FIG. 4: $(m, n) = (2, 1)$: Mean-field period $T(E)$ divided by 2π (red line) and many-particle density of states (histogram) for $N = 9000$ particles for $v = 1$ and $\epsilon = 0.5$ (left) and $\epsilon = 1.5$ (right).

with the expected solution $p = -\frac{1}{2}$ and two solutions of the quadratic equation, where one of them is in the interval $-\frac{1}{2} \leq p \leq \frac{1}{2}$ and the second one only in the subcritical case [1, 14]. The x -component can be determined by $s_x = v f(p)/\epsilon$. In the supercritical case, where only the two fixed points at the poles exist, both of them are centers, otherwise the one at the south pole is a saddle point, whereas the other two are centers. At the south pole the slope of $f(p)$ is equal to -2 , so that the eigenvalue (74) of the stability matrix is $\lambda = \pm\sqrt{-\epsilon^2 + 2v^2}$, which again yields a center in the supercritical case and a saddle point in the subcritical regime. Detailed numerical examples can be found in [1]. The mean-field energies at the fixed points are shown in figure 3 and compared with the quantum eigenvalues for $N = 80$ particles ($N_{\text{dim}} = 41$), which are clearly organized by the classical fixed point energies. (Note that the mean-field energies E must be rescaled by a factor $\eta = 1/N_{\text{dim}}$.)

Figure 4 shows the mean-field period $T(E)/2\pi$ as well as a histogram of the many-particle eigenvalues (scaled by a factor η) for $N = 9000$ particles for $v = 1$ in the sub- and supercritical region. The density of states is in excellent agreement with the mean-field period. At the boundaries of the allowed energy interval it is equal to the reciprocal period at the centers. In the subcritical case, there is a divergence at the energy $-\epsilon/2$ at the south pole in the limit $N \rightarrow \infty$. Such a level bunching at the classical saddle point energy in this limit can be related to a quantum phase transition [6, 14].

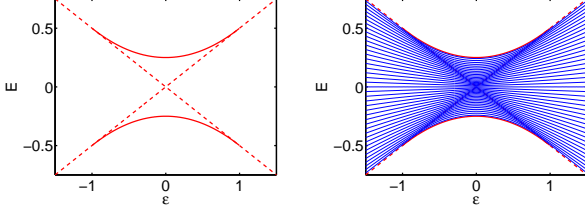


FIG. 5: $(m, n) = (2, 2)$: Mean-field fixed point energies (red) and (scaled) many-particle energies (blue) in dependence of ϵ for $v = 1$ and $N = 160$ particles.

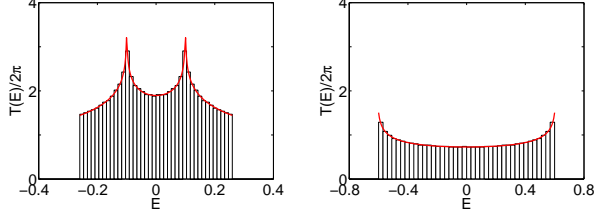


FIG. 6: $(m, n) = (2, 2)$: Mean-field period $T(E)$ divided by 2π (red line) and many-particle density of states (histogram) for $N = 9000$ particles for $v = 1$ and $\epsilon = 0.2$ (left) and $\epsilon = 1.2$ (right).

(3) For the case $m = n = 2$ we have

$$r(p) = \frac{1}{4} - p^2, \quad f(p) = 2p\left(\frac{1}{4} - p^2\right) \quad (82)$$

and the fixed points are found from (76) as

$$p = \pm \frac{\epsilon}{2v}, \quad s_x = \frac{v}{\epsilon} f(p) = \pm \frac{1}{4} \left(1 - \frac{\epsilon^2}{v^2}\right) \quad (83)$$

for $\epsilon^2 < v^2$. These fixed points are centers and the fixed points at the poles are saddles. For $\epsilon^2 > v^2$ we find only two centers at the poles. The energy at the fixed points (83) is

$$E_{1,2} = \pm \frac{v}{4} \left(1 + \frac{\epsilon^2}{v^2}\right) \quad (84)$$

a curve, that joins smoothly with the energies $E_{\pm} = \pm \epsilon/2$ at the critical values $\epsilon = \pm v$. Figure 5 shows the mean-field energies at the fixed points and the quantum eigenvalues for $N = 160$ particles ($N_{\text{dim}} = 41$), which are again supported by the classical skeleton of fixed point energies.

Histograms of the many-particle eigenvalues are shown in figure 6 for $N = 9000$ particles for $v = 1$ in comparison with the mean-field periods, again in the sub- and supercritical regions. Because of $m = n$ the distributions are symmetric. For $\epsilon = 0.2$ there are two saddle points at the poles, and hence two singularities, and for $\epsilon = 1.2$ we only have two centers at the poles with frequency $\omega = \sqrt{(v^2 - \epsilon^2)/2}$ (see (75)).

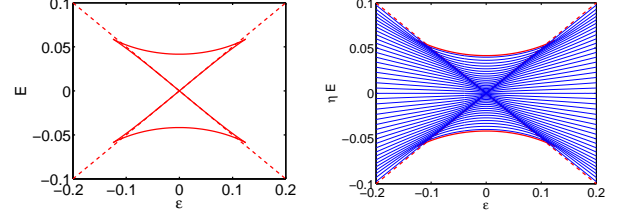


FIG. 7: $(m, n) = (3, 3)$: Mean-field fixed point energies (red) and (scaled) many-particle energies (blue) in dependence of ϵ for $v = 1$ and $N = 360$ particles.

(4) The case $(m, n) = (3, 3)$ is more involved. First we have

$$r(p) = \frac{1}{3} \left(\frac{1}{4} - p^2\right)^{3/2}, \quad f(p) = \frac{1}{3} p \left(\frac{1}{4} - p^2\right)^2 \quad (85)$$

and the fixed points are found from (76), a second order polynomial in p^2 , as

$$p = \pm \sqrt{\frac{1}{8} \left(1 \pm \sqrt{1 - (8\epsilon/v)^2}\right)}, \quad s_x = \frac{v}{\epsilon} f(p) \quad (86)$$

for $(8\epsilon)^2 < v^2$. Note that here we have four fixed points in addition to the poles, which is the maximum number possible, as discussed above. This transcritical bifurcation occurs for $\epsilon = 0$ at the degenerate fixed points located at the poles.

Figure 7 shows the energies at the six fixed points in dependence of ϵ . The four non-trivial ones trace out a double swallowtail curve with four cusps at the critical values $\epsilon_c = \pm v/8$ with energy $E = \pm v/12\sqrt{2} = \pm \sqrt{2}\epsilon/3$, which is slightly smaller than the energy $\pm \epsilon/2$ at the poles. The fixed points close to the line $\pm \epsilon$ are saddle points, those on the curved lines passing through $E = \pm v/24$ for $\epsilon = 0$ are centers. At the cusps the character changes, which can also be seen from the vanishing of the eigenvalues of the Jacobi matrix (74). Again, as demonstrated in figure 7 for $N = 320$ particles ($N_{\text{dim}} = 41$), the classical fixed point energies provide a skeleton for the quantum eigenvalues.

It is instructive to have a look at the potential curves $U_{\pm}(p)$ defined in (71) and shown in figure 8 for $v = 1$ and selected values of ϵ . For $\epsilon = 0.08$ we are in the subcritical region and the potential $U_{-}(p)$ has a minimum and a very shallow maximum, which is hard to identify in the plot, but it must necessarily exist because the slope of both potentials $U_{\pm}(p)$ at $p = -\frac{1}{2}$ is equal to ϵ , i.e. positive. This shallow maximum with energy $E_{\text{max-}}$ appears as a fixed point of the dynamics, a saddle point with energy E_{-} , and the minimum with energy $E_{\text{min-}}$ as a center. The same is true, of course, for the potential curve $U_{+}(p)$ with a saddle energy E_{+} , a maximum $E_{\text{max+}}$ and a minimum $E_{\text{min+}}$. At the critical value $\epsilon_c = v/8$ the minimum and the maximum coalesce and disappear for larger values of ϵ .

In the subcritical region $|\epsilon| < \epsilon_c$ there exist two disconnected allowed potential regions in the energy intervals

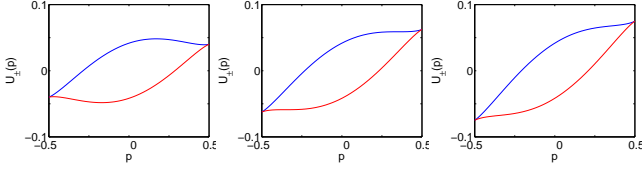


FIG. 8: $(m, n) = (3, 3)$: Potentials $U_+(p)$ (blue) and $U_-(p)$ (red) for $v = 1$ and $\epsilon = 0.08, 0.125, 0.15$ (from left to right).

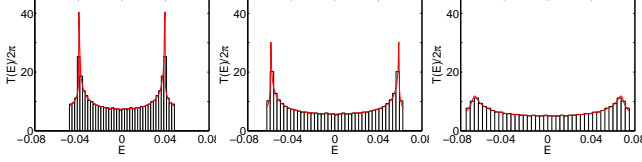


FIG. 9: $(m, n) = (3, 3)$: Mean-field period $T(E)$ divided by 2π (red line) and many-particle density of states (histogram) for $N = 9000$ particles for $v = 1$ and $\epsilon = 0.08, 0.125, 0.15$ (from left to right).

$E_- < E < E_{\max-}$ and $E_{\min+} < E < E_+$, both contributing to the mean-field density of states (70), which therefore shows four steps at the energies of the minima and maxima and two logarithmic singularities at the energies of the saddle points. Figure 9 shows histograms of the state density and mean-field periods for $v = 1$ and selected values of ϵ in different regions. The case $\epsilon = 0.08$ is in the subcritical region discussed above, for the critical value $\epsilon = 0.125$ the minima and maxima coincide with the saddle point, shown as two singularities of the mean-field period, which disappear in the supercritical regime. Here, however, they are still observable as peaks in the vicinity of the former singularities, as shown in the figure for $\epsilon = 0.15$. With increasing ϵ these maxima decrease.

Let us finally explore the subcritical case $\epsilon = 0.08$ in more detail to resolve the structure of the state densities in this regime. A magnification of the neighborhood of

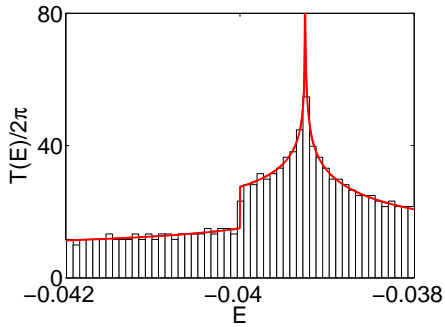


FIG. 10: $(m, n) = (3, 3)$: Magnification of the vicinity of the left singularity in figure 9 for $\epsilon = 0.08$, however for $N = 72000$ particles.

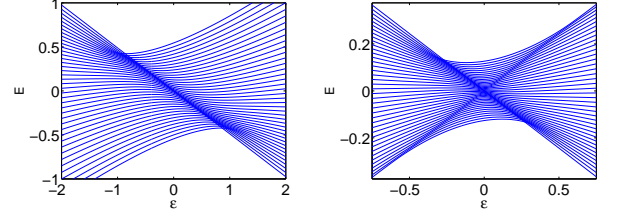


FIG. 11: Many-particle (scaled) energies in dependence of ϵ for $v = 1$ and $(m, n) = (3, 1)$ (left, $N = 120$ particles) and $(m, n) = (3, 2)$ (right, $N = 240$ particles).

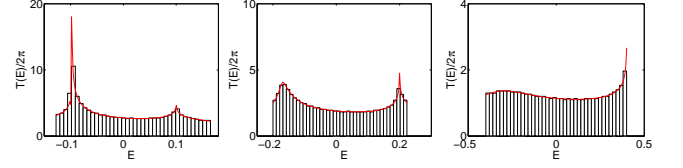


FIG. 12: $(m, n) = (3, 2)$: Mean-field period $T(E)$ divided by 2π (red line) and many-particle density of states (histogram) for $N = 9000$ particles for $v = 1$ and $\epsilon = 0.2, 0.4, 0.8$ from left to right.

the singularity in figure 9 (left panel) is shown in figure 10, however for $N = 72000$ particles, where we clearly observe the step at $E_- = 0.04$ in addition to the singularity at the saddle point energy $E_{\max-}$ in the quantum density of states.

(5) Finally we will briefly consider the cases $(m, n) = (3, 1)$ and $(3, 2)$ whose energy eigenvalues are shown in figure 11 for $N = 120$ or 240 particles. Their structure should be understandable now without presenting their classical skeleton.

The figure on the left, for $(3, 1)$, is a combination of the structures already shown in figures 3 and 7 for $(m, n) = (2, 1)$ and $(3, 3)$, respectively. At the north pole the Kummer surface is smooth and generates no bifurcation. At the south pole we find a cusp, leading to a cusp singularity as in the case $(3, 3)$ showing up in the upper left and lower right of the (E, ϵ) -plane.

The figure on the right, for $(3, 2)$, also combines features discussed before. Again we observe the cusps on the upper left and lower right, but here we also have a tip of the Kummer surface at the north pole, giving rise to a bifurcation and the additional line $E = \epsilon/2$ as already seen in figures 5 and 7. The multi-particle densities are shown in figure 12 along with the mean-field periods in different parameter regions ($\epsilon = 0.2, 0.4$ and 0.8). One of the two singularities for $\epsilon = 0.2$ changes into a maximum for $\epsilon = 0.4$ and for $\epsilon = 0.8$ also the second singularity disappeared.

V. SUMMARY AND OUTLOOK

The mean-field approximation is quite often indispensable in studies of multi-particle quantum systems. In addition, as demonstrated above for simple types of particle conversion systems, it also offers illuminating tools for understanding the characteristic features of quantum systems. The energy spectra, for example, are clearly supported by the skeleton of mean-field fixed points, showing up, e.g., as boundaries, steps of singularities of the quantum state densities in the thermodynamic limit of large particle numbers.

In addition, the present analysis is based on polynomially deformed algebras, where an interesting connection between quantum (commutator) algebras and classical (Poisson bracket) ones appeared. The observed differences deserve further studies. It should also be noted that the transition from quantum to mean-field, the ‘classicalization’, employed here is quite heuristic and deserves a more sophisticated treatment, for example in terms of coherent states for deformed algebras as already pointed out in [1].

Finally, the present study concentrated on the spectral features of the conversion systems. A comparison of quantum and mean-field dynamics will also be of interest and corresponding investigations based on semiclassical phase space densities [41] will be presented in future publications.

Appendix A: Polynomial deformations of $su(2)$

The deformed algebra is generated by the three elements $\hat{J}_0 = \hat{J}_0^\dagger$, $\hat{J}_+ = \hat{J}_-^\dagger$ satisfying

$$[\hat{J}_0, \hat{J}_\pm] = \pm \hat{J}_\pm, \quad [\hat{J}_+, \hat{J}_-] = 2\hat{F}(\hat{J}_0), \quad (\text{A1})$$

where $[\cdot, \cdot]$ is the commutator, and $\hat{F}(\hat{J}_0) = \sum_{j=0}^k \alpha_j \hat{J}_0^j$ is a polynomial of order k . For $\hat{F}(\hat{J}_0) = \hat{J}_0$ we have $[\hat{J}_+, \hat{J}_-] = 2\hat{J}_0$, i.e. the Lie algebra $su(2)$, so that we have a polynomial deformation of $su(2)$. It can be shown that the Casimir operator is given by

$$\hat{C} = \hat{J}_- \hat{J}_+ + \hat{\phi}(\hat{J}_0) \quad (\text{A2})$$

where $\hat{\phi}(\hat{J}_0)$ is a polynomial in \hat{J}_0 of order $k+1$ with $\hat{\phi}(0) = 0$, which can be expressed in terms of Bernoulli

functions $B_n(z)$ and Bernoulli numbers $B_n = B_n(0)$ as

$$\hat{\phi}(\hat{J}_0) = 2 \sum_{j=0}^k \frac{(-1)^{j+1}}{j+1} \alpha_j (B_{j+1}(-\hat{J}_0) - B_{j+1}), \quad (\text{A3})$$

related to $\hat{F}(\hat{J}_0)$ by

$$\hat{F}(\hat{J}_0) = \frac{1}{2}(\hat{\phi}(\hat{J}_0) - \hat{\phi}(\hat{J}_0 - 1)). \quad (\text{A4})$$

(see, e.g., [28] and references therein). Up to third order, $k=3$, (A3) yields

$$\begin{aligned} \hat{\phi}(\hat{J}_0) = & \left(2\alpha_0 + \alpha_1 + \frac{\alpha_2}{3}\right) \hat{J}_0 + \left(\alpha_1 + \alpha_2 + \frac{\alpha_3}{2}\right) \hat{J}_0^2 \\ & + \left(\frac{2\alpha_2}{3} + \alpha_3\right) \hat{J}_0^3 + \frac{\alpha_3}{2} \hat{J}_0^4 \end{aligned} \quad (\text{A5})$$

(see also [30, 31]). Alternatively, with

$$\hat{J}_x = \frac{1}{2}(\hat{J}_+ + \hat{J}_-), \quad \hat{J}_y = \frac{1}{2i}(\hat{J}_+ - \hat{J}_-), \quad \hat{J}_z = \hat{J}_0, \quad (\text{A6})$$

and

$$[\hat{J}_y, \hat{J}_z] = i\hat{J}_x, \quad [\hat{J}_z, \hat{J}_x] = i\hat{J}_y, \quad [\hat{J}_x, \hat{J}_y] = i\hat{F}(\hat{J}_z) \quad (\text{A7})$$

the Casimir (A2) is written as

$$\hat{C} = \hat{J}_x^2 + \hat{J}_y^2 - \hat{F}(\hat{J}_z) + \hat{\phi}(\hat{J}_z) = \hat{J}_x^2 + \hat{J}_y^2 + \frac{1}{2}(\hat{\phi}(\hat{J}_z) + \hat{\phi}(\hat{J}_z - 1)). \quad (\text{A8})$$

For polynomials up to third order (A5) implies

$$\begin{aligned} \hat{C} = & \hat{J}_x^2 + \hat{J}_y^2 - \alpha_0 + \left(2\alpha_0 + \frac{\alpha_2}{3}\right) \hat{J}_z \\ & + \left(\alpha_1 + \frac{\alpha_3}{2}\right) \hat{J}_z^2 + \frac{2\alpha_2}{3} \hat{J}_z^3 + \frac{\alpha_3}{2} \hat{J}_z^4. \end{aligned} \quad (\text{A9})$$

For the linear case $\hat{F}(\hat{J}_z) = \hat{J}_z$ we have $\hat{\phi}(\hat{J}_z) = \hat{J}_z + \hat{J}_z^2$ and $\hat{C} = \hat{J}_x^2 + \hat{J}_y^2 + \hat{J}_z^2$.

It should be noted that these results are only valid for the commutator and not for the Poisson bracket (see the footnote in [17]).

Acknowledgments

The author thanks Eva-Maria Graefe and Kevin Rappadius for valuable comments on the manuscript.

-
- [1] E. M. Graefe, M. Graney, and A. Rush, Phys. Rev. A **92** (2015) 012121
 - [2] V. P. Karassiov and A. B. Klimov, Phys. Lett. A **191** (1998) 117
 - [3] A. Vardi, V. A. Yurovsky, and J. R. Anglin, Phys. Rev. A **64** (2001) 063611
 - [4] V. P. Karassiov, A. A. Gusev, and S. I. Vinitsky, Phys.

- Lett. A **295** (2002) 247
- [5] H.-Q. Zhou, J. Links, and R. H. McKenzie, Int. J. Mod. Phys. B **17** (2003) 5819
- [6] G. Santos, A. Tonel, A. Foerster, and J. Links, Phys. Rev. A **73** (2006) 023609
- [7] J. Li, D.-F. Ye, C. Ma, L.-B. Fu, and J. Liu, Phys. Rev. A **79** (2009) 025602

- [8] J. Liu and B. Liu, *Front. Phys. China* **5** (2010) 123
- [9] C. Khripkov and A. Vardi, *Phys. Rev. A* **84** (2011) 021606
- [10] S.-C. Li and L.-B. Fu, *Phys. Rev. A* **84** (2011) 023605
- [11] G. Santos, *J. Phys. A* **44** (2011) 345003
- [12] B. Cui, L. C. Wang, and X. X. Yi, *Phys. Rev. A* **85** (2012) 013618
- [13] H. Z. Shen, X.-M. Xiu, and X. X. Yi, *Phys. Rev. A* **87** (2013) 063613
- [14] P. Pérez-Fernández, P. Cejnar, J. M. Arias, J. Dukelsky, J. E. García-Ramos, and A. Relaño, *Phys. Rev. A* **83** (2011) 033802
- [15] E. A. Donley, N. R. Claussen, S. T. Thompson, and C. E. Wieman, *Nature* **417** (2002) 529
- [16] A. Relaño, J. Dukelsky, P. Pérez-Fernández, and J. M. Arias, *Phys. Rev. E* **90** (2014) 042139
- [17] M. Roček, *Phys. Lett. B* **255** (1990) 554
- [18] A. P. Polychronakos, *Mod. Phys. Lett. A* **5** (1990) 2325
- [19] D. Bonatsos, P. Kolokotronis, C. Daskaloyannis, A. Ludu, and C. Quesne, *Czech. J. Phys.* **46** (1996) 1189
- [20] Y.-H. Lee, W.-L. Yang, and Y.-Z. Zhang, *J. Phys. A* **43** (2010) 185204
- [21] D. D. Holm, *Geometric Mechanics Part I: Dynamics and Symmetry*, Imperial College Press, London, 2011
- [22] D. D. Holm and C. Vizman, *J. Geom. Mech.* **4** (2012) 297
- [23] M. Kummer, *Comm. Math. Phys.* **48** (1976) 53
- [24] M. Kummer, *Comm. Math. Phys.* **58** (1978) 85
- [25] M. Kummer, *Indiana Univ. Math. J.* **30** (1981) 281
- [26] M. Kummer, in *Local and Global Methods in Nonlinear Dynamics, Lecture notes in Physics, Vol. 252*, edited by A. V. Sáenz, page 19. Springer, New York, 1986
- [27] M. Kummer, *J. Diff. Eq* **83** (1990) 220
- [28] C. Delbecq and C. Quesne, *J. Phys. A* **26** (1993) L127
- [29] N. Debergh, *J. Phys. A* **31** (1998) 4013
- [30] N. Debergh, *J. Phys. A* **33** (2000) 7109
- [31] J. Beckers, *Proceedings of Institute of Mathematics of NAS of Ukraine* **30** (2000) 275
- [32] J. Links, H.-Q. Zhou, R. H. McKenzie, and M. D. Gould, *J. Phys. A* **36** (2003) R63
- [33] A. Odziejewicz, in *Int. Conf: Quantum control, exact perturbative, linear or nonlinear*, 2014. see http://pluton.fis.cinvestav.mx/Bogdan50/2014Meksyk_Kummer.pdf
- [34] D. D. Holm, *Geometric Mechanics Part II: Rotating, Translating and Rolling*, Imperial College Press, London, 2011
- [35] E. M. Graefe and H. J. Korsch, *Phys. Rev. A* **76** (2007) 032116
- [36] F. Nissen and J. Keeling, *Phys. Rev. A* **81** (2010) 063628
- [37] L. Simon and W. T. Strunz, *Phys. Rev. A* **86** (2012) 053625
- [38] V. I. Arnold, *Ordinary differential equations*, Springer, Berlin, New York, 2006
- [39] E.-M. Graefe, H. J. Korsch, and M. P. Strzys, *J. Phys. A* **47** (2014) 085304
- [40] J. H. Wilkinson, *The Algebraic Eigenvalue Problem*, Oxford University Press, Oxford, 1965
- [41] F. Trimborn, D. Witthaut, and H. J. Korsch, *Phys. Rev. A* **77** (2008) 043631